



Knockdown of the mitochondria-localized protein p13 protects against experimental parkinsonism

Naoki Inoue^{1,2,3}, Sae Ogura¹, Atsushi Kasai¹, Takanobu Nakazawa^{1,4}, Kazuya Ikeda¹, Shintaro Higashi¹, Ayako Isotani^{5,6}, Kousuke Baba⁷, Hideki Mochizuki⁷, Harutoshi Fujimura⁸, Yukio Ago¹, Atsuko Hayata-Takano^{1,9}, Kaoru Seiriki^{1,2}, Yusuke Shintani¹, Norihito Shintani^{1,*}  & Hitoshi Hashimoto^{1,9,10,11,**} 

Abstract

Mitochondrial dysfunction in the nigrostriatal dopaminergic system is a critical hallmark of Parkinson's disease (PD). Mitochondrial toxins produce cellular and behavioural dysfunctions resembling those in patients with PD. Causative gene products for familial PD play important roles in mitochondrial function. Therefore, targeting proteins that regulate mitochondrial integrity could provide convincing strategies for PD therapeutics. We have recently identified a novel 13-kDa protein (p13) that may be involved in mitochondrial oxidative phosphorylation. In the current study, we examine the mitochondrial function of p13 and its involvement in PD pathogenesis using mitochondrial toxin-induced PD models. We show that p13 overexpression induces mitochondrial dysfunction and apoptosis. p13 knockdown attenuates toxin-induced mitochondrial dysfunction and apoptosis in dopaminergic SH-SY5Y cells via the regulation of complex I. Importantly, we generate p13-deficient mice using the CRISPR/Cas9 system and observe that heterozygous p13 knockout prevents toxin-induced motor deficits and the loss of dopaminergic neurons in the substantia nigra. Taken together, our results suggest that manipulating p13 expression may be a promising avenue for therapeutic intervention in PD.

Keywords cell death; complex I; mitochondria; p13; Parkinson's disease

Subject Categories Molecular Biology of Disease; Neuroscience

DOI 10.15252/embr.201744860 | Received 19 July 2017 | Revised 15 December 2017 | Accepted 21 December 2017 | Published online 25 January 2018

EMBO Reports (2018) 19: e44860

See also: **JS Valadas & P Verstreken** (March 2018)

Introduction

Parkinson's disease (PD), one of the most common motor disorders, is caused by the progressive and specific loss of nigrostriatal dopaminergic neurons [1,2]. Dopamine modulators are first-line therapeutics for PD, but they face tolerability issues and have limited efficacy [3]. Therefore, there is a compelling need for novel therapeutic strategies for PD [4–6].

Although the aetiology of PD remains unclear, the involvement of mitochondrial dysfunction in PD has been increasingly convincing [7–10]. Mitochondrial complex I deficiencies are detected in postmortem nigrostriatal tissues of patients with PD [11–13]. Inhibitors of mitochondrial complex I such as rotenone and 1-methyl-4-tetramethyl-*p*-phenylenediamine (MPTP) induce several hallmarks of PD, including motor deficits and nigrostriatal dopaminergic cell death in rodents and primates [14–16]. Furthermore, mutations in mitochondrial DNA (mtDNA) leading to mitochondrial dysfunction have been considered a risk factor for PD [17,18]. The current model of PD proposes that defects in PTEN-induced putative kinase 1 (PINK1) and Parkin, well-known causative gene products for familial PD, cause an accumulation of dysfunctional mitochondria [19,20]. These findings argue that maintaining mitochondrial integrity could be a powerful and convincing strategy for PD treatment.

We have recently identified a novel 13-kDa protein named p13, whose expression is decreased in pancreatic islets exposed to oxidative

1 Laboratory of Molecular Neuropharmacology, Graduate School of Pharmaceutical Sciences, Osaka University, Suita, Osaka, Japan

2 Interdisciplinary Program for Biomedical Sciences, Institute for Academic Initiatives, Osaka University, Suita, Osaka, Japan

3 Research Fellowships for Young Scientists of the Japan Society for the Promotion of Science, Chiyoda, Tokyo, Japan

4 Department of Pharmacology, Graduate School of Dentistry, Osaka University, Suita, Osaka, Japan

5 Animal Resource Center for Infectious Diseases, Immunology Frontier Research Center, Osaka University, Suita, Osaka, Japan

6 Graduate School of Biological Sciences, Nara Institute of Science and Technology, Ikoma, Nara, Japan

7 Department of Neurology, Graduate School of Medicine, Osaka University, Suita, Osaka, Japan

8 Toneyama National Hospital, Toyonaka, Osaka, Japan

9 Molecular Research Center for Children's Mental Development, United Graduate School of Child Development, Osaka University, Kanazawa University, Hamamatsu University School of Medicine, Chiba University and University of Fukui, Suita, Osaka, Japan

10 iPS Cell-based Research Project on Brain Neuropharmacology and Toxicology, Graduate School of Pharmaceutical Sciences, Osaka University, Suita, Osaka, Japan

11 Division of Bioscience, Institute for Data Biology Science, Osaka University, Suita, Osaka, Japan

*Corresponding author. Tel: +81 6 6879 8181; E-mail: shintani@phs.osaka-u.ac.jp

**Corresponding author. Tel: +81 6 6879 8180; E-mail: hashimoto@phs.osaka-u.ac.jp

stress by a high-fat diet [21]. Oxidative stress is caused by the excessive accumulation of reactive oxygen species generated in dysfunctional mitochondria [22,23]. Recent proteomic analysis has identified human p13 (C7orf55) as a novel protein that may interact with mitochondrial proteins such as NDUFB1, a complex I subunit, and ATPAF2, a complex V subunit [24]. Furthermore, p13 has been demonstrated to partially co-localize with mtDNA by immunostaining [25]. We therefore hypothesized that p13 is a regulator of mitochondrial function. However, the mitochondrial function of p13 and its involvement in the molecular pathogenesis of PD are currently unknown.

In the present study, we examined the roles of p13 in mitochondrial function in both *in vitro* and *in vivo* PD models. Our results suggest that the reduction in p13 expression acts as a protective factor against PD pathogenesis via the maintenance of mitochondrial function.

Results and Discussion

p13 overexpression exacerbates rotenone-induced mitochondrial dysfunction and apoptosis in SH-SY5Y cells

We found that p13 was co-localized with Hsp60, a mitochondrial matrix-localized protein in SH-SY5Y cells, a human neuroblastoma cell line (Fig 1A). Next, we measured mitochondrial membrane potential ($\Delta\Psi_m$) using tetramethylrhodamine ethyl ester perchlorate (TMRE), which is sensitive to $\Delta\Psi_m$. We found that p13 overexpression significantly decreased $\Delta\Psi_m$ compared with the levels measured in mock-infected cells (Fig 1B). The $\Delta\Psi_m$ decrease induced by rotenone, a mitochondrial complex I inhibitor, was exacerbated in p13-overexpressed SH-SY5Y cells (Fig 1B). The signal of MitoTracker Green FM, which localizes to mitochondria regardless of $\Delta\Psi_m$, did not differ between mock- and p13-overexpressed cells under basal or rotenone-treated conditions (Fig 1C), suggesting that p13 overexpression does not affect mitochondrial mass. Because mitochondria play a key role in apoptosis [26,27], we evaluated the effects of p13 overexpression on apoptosis induction by measuring the levels of cleavage of poly (ADP-ribose) polymerase (PARP). We observed that p13 overexpression significantly increased the levels of PARP cleavage in both the vehicle- and the rotenone-treated cells (Fig 1D). We also applied the terminal deoxynucleotidyl transferase (TdT)-mediated deoxyuridine triphosphate (dUTP) nick-end labelling (TUNEL) method to detect apoptotic cells. We found that the overexpression of p13 increased the number of TUNEL-positive cells under basal conditions and exacerbated the rotenone-induced increase in TUNEL-positive cells (Fig 1E). These data demonstrate that p13 overexpression induces mitochondrial dysfunction and apoptosis in SH-SY5Y cells.

p13 knockdown prevents parkinsonian toxicant-induced mitochondrial dysfunction and apoptosis in SH-SY5Y cells

We first performed subcellular fractionation experiments and observed that endogenous p13 was most abundant in the mitochondria-enriched fraction (Figs 2A and EV4B). Furthermore, to characterize the intramitochondrial localization of endogenous p13, we used digitonin fractionation, in which mitochondria were treated with various concentrations of digitonin for progressive membrane solubilization. We found that p13 showed a similar resistance to digitonin compared with the mitochondrial matrix marker Hsp60 (Fig 2B). Tom20 and Tim23, which are mitochondrial outer and inner membrane markers, respectively, are more sensitive to higher concentrations of digitonin than p13 or Hsp60 is (Fig 2B). These results suggest that p13 is mainly localized in the mitochondrial matrix. Based on the results from the overexpression experiments (Fig 1), we hypothesized that the downregulation of p13 expression prevents stress-induced mitochondrial dysfunction and apoptosis. We confirmed shRNA-mediated p13 knockdown in SH-SY5Y cells (Fig EV1A and B). We then evaluated the effects of p13 knockdown on rotenone-induced mitochondrial dysfunction and apoptosis in SH-SY5Y cells. In contrast to control knockdown, p13 knockdown significantly prevented the rotenone-induced decrease in $\Delta\Psi_m$ and increases in cleaved PARP and TUNEL-positive cells (Fig 2C–E). In the basal condition, the p13 knockdown did not affect the fluorescence intensity of TMRE, the cleavage of PARP or the percentage of TUNEL-positive cells (Fig 2C–E). Similar results were obtained using another shRNA construct (p13 shRNA #2) targeting a different region of p13 (Fig EV1C–E). Furthermore, p13 knockdown attenuated the decrease in $\Delta\Psi_m$ and the release of lactate dehydrogenase (LDH), a marker of cell death, by the mitochondrial complex I inhibitor 1-methyl-4-phenylpyridine (MPP⁺), a metabolite of MPTP (Fig EV1G and H), confirming the protective effects of p13 knockdown against complex-I-inhibitor-induced toxicity. In addition to the toxin-induced PD model, we also examined the effects of p13 knockdown using a non-toxic PD model in which PINK1 was knocked down (Fig EV1I) and found that p13 knockdown significantly prevented the decrease in $\Delta\Psi_m$ and the PARP cleavage in the PINK1-knockdown cells (Fig EV1J and K). Importantly, in rescue experiments (Fig 2F and G), the restoration of p13 expression in p13-knockdown cells significantly reversed the protective effects of p13 knockdown on PARP cleavage by rotenone (Fig 2G), but the effect of the restoration of p13 expression on the rotenone-induced decrease in $\Delta\Psi_m$ was modest (Fig 2F). These data suggest that p13 knockdown significantly prevents parkinsonian toxicant-induced mitochondrial dysfunction and apoptosis in SH-SY5Y cells.

Figure 1. p13 overexpression exacerbates rotenone-induced mitochondrial dysfunction and apoptosis in SH-SY5Y cells.

- A Co-localization of overexpressed p13 and Hsp60, a mitochondrial matrix protein, in p13-infected cells. Nucleus was stained with Hoechst (blue). Scale bars, 10 μ m.
 B, C Exacerbated rotenone-induced decrease in $\Delta\Psi_m$ but no change in mitochondrial mass in p13-infected cells. $\Delta\Psi_m$ and mitochondrial mass were determined by measuring the fluorescence levels of TMRE (B) and MitoTracker Green FM (C), respectively.
 D, E Exacerbated rotenone-induced apoptosis in p13-infected cells. Apoptosis levels were evaluated by measuring the increases in PARP cleavage (D) and in percentage of TUNEL-positive cells (E). The levels of cleaved PARP were normalized to those of β -actin (D). The percentage of TUNEL-positive cells was determined by TUNEL (green) and Hoechst (blue, a nuclear marker) staining (E). Representative images (left) and their quantification (right) were shown. Scale bar, 50 μ m.

Data information: In all experiments, cells were infected with lentiviral vectors expressing mock or FLAG-tagged p13 (p13 o/e). Seventy-two hours after infection, cells were exposed to vehicle or 100 nM rotenone for 24 h (B–E). p13 was detected using an antibody against p13. All data are presented as the mean \pm SEM ($n = 3$).

* $P < 0.05$, ** $P < 0.01$ by the Tukey–Kramer test.

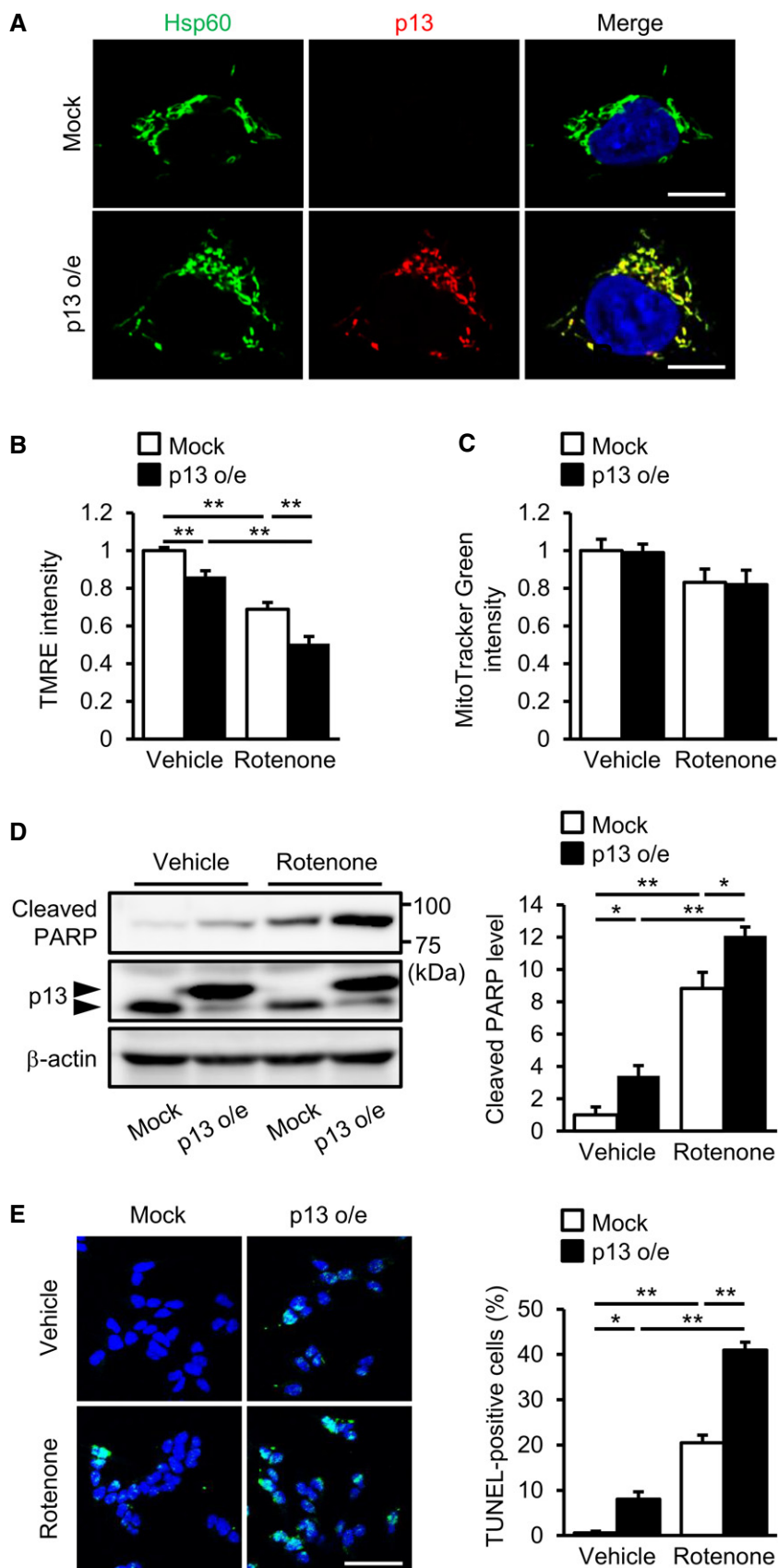


Figure 1.

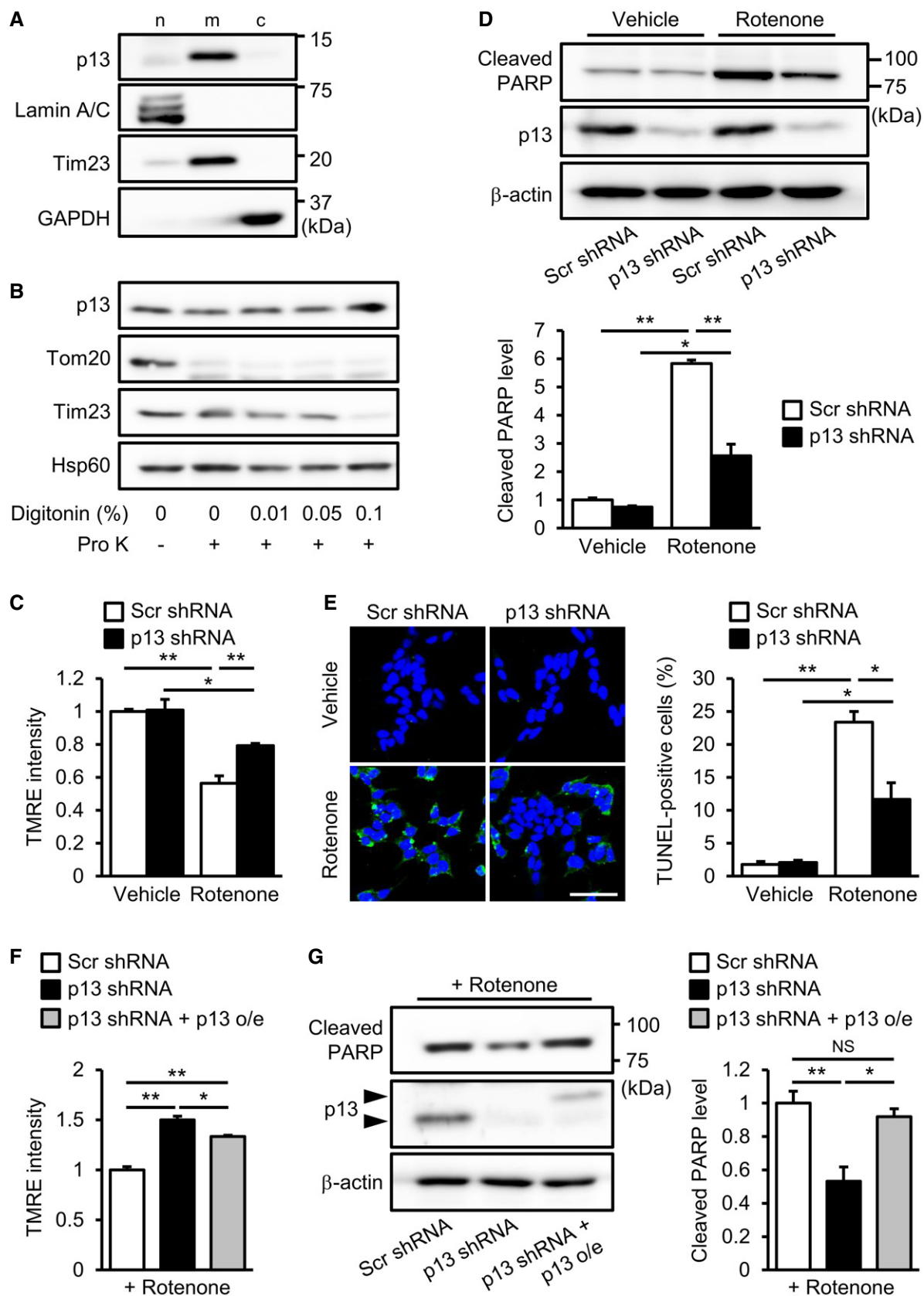


Figure 2.

Figure 2. p13 knockdown prevents rotenone-induced mitochondrial dysfunction and apoptosis in SH-SY5Y cells.

- A Distribution of p13 in the nuclear (n)-, mitochondria (m)- and cytosol (c)-enriched fractions of SH-SY5Y cells. The blot was probed with antibodies against p13, Lamin A/C (a nuclear marker), Tim23 (a mitochondrial marker) and GAPDH (a cytoplasmic marker).
- B Mitochondrial localization of p13 in SH-SY5Y cells. Isolated mitochondria were treated with 20 $\mu\text{g/ml}$ proteinase K (Pro K) in the absence or presence of increasing concentrations of digitonin (0.01, 0.05 and 0.1%). Samples were subjected to Western blotting with antibodies against p13, Tom20 (outer mitochondrial membrane marker), Tim23 (inner mitochondrial membrane marker) and Hsp60 (mitochondrial matrix marker).
- C–E Prevention of the rotenone-induced decrease in $\Delta\Psi\text{m}$ (C), increase in PARP cleavage (D) and increase in percentage of TUNEL-positive cells (E) in p13 shRNA-infected cells. Scale bar, 50 μm .
- F, G Attenuation of the rotenone-induced decrease in $\Delta\Psi\text{m}$ (F) and increase in PARP cleavage (G) by the restoration of p13 expression in p13 shRNA-infected cells. Arrowheads showed FLAG-tagged p13 (p13 o/e) and endogenous p13.

Data information: Seventy-two hours after infection with lentiviral vectors expressing scrambled shRNA (Scr shRNA) or p13 shRNA, cells were exposed to vehicle or 100 nM rotenone for 24 h (C–G). $\Delta\Psi\text{m}$ was determined by measuring the TMRE fluorescence levels (C, F). The levels of cleaved PARP were normalized to those of β -actin (D, G). The percentage of TUNEL-positive cells was determined by TUNEL (green) and Hoechst (blue, a nuclear marker) staining (E). Representative images (upper, D; left, E, G) and their quantification (lower, D; right, E, G) were shown. All data are presented as the mean \pm SEM ($n = 3$). * $P < 0.05$, ** $P < 0.01$ by the Tukey–Kramer test. NS, not significant.

Currently, it is unclear why, in contrast to p13 overexpression, p13 knockdown did not affect the fluorescence intensity of TMRE and the cleavage of PARP in the basal condition. We assume, however, several possibilities to reconcile the discrepancy. (i) A small amount of residual p13 protein after p13 knockdown may keep mitochondrial function in the basal condition. (ii) Other mitochondrial factors may compensate for the effect of p13 knockdown in the basal condition.

p13 knockdown maintains complex I activity independently of PINK1-associated autophagy in rotenone-treated SH-SY5Y cells

Recent reports have shown that p13 may interact with mitochondrial complex I and mtDNA [24,25]; however, it is unclear whether p13 is involved in their functions. We first examined the effects of p13 knockdown on complex I activity in the rotenone-treated SH-SY5Y cells. Interestingly, p13 knockdown significantly prevented the rotenone-induced decrease in complex I activity compared with that observed in scrambled shRNA-infected cells (Figs 3A and EV1F). We next examined the co-immunoprecipitation study and found that the overexpressed p13 co-precipitated well with complex I, as revealed by an immunoblot for nicotinamide adenine dinucleotide dehydrogenase (ubiquinone) 1 β subcomplex 8 (NDUFB8), a mitochondrial complex I subunit, in SH-SY5Y cells (Fig 3B). Endogenous p13 also co-precipitated with complex I proteins in SH-SY5Y cells (Fig 3C). Immunocytochemistry showed that the overexpressed p13 was co-localized with mitochondrial complex I (Fig EV2A). We then examined the effects of p13 knockdown on complex I assembly in SH-SY5Y cells and found that p13 knockdown prevented the rotenone-induced impairment of complex I assembly (Fig 3D). We then examined the expression levels of mitochondrial mRNAs encoded by mtDNA in p13-knockdown rotenone-treated SH-SY5Y cells. There was no significant difference in mitochondrial mRNA expression levels between scrambled shRNA- and p13 shRNA-infected rotenone-treated SH-SY5Y cells (Fig EV2B). These results suggest that the interaction between p13 and complex I but not mtDNA is necessary to prevent mitochondrial dysfunction.

A popular topic in PD pathogenesis research is PINK1/Parkin-mediated autophagy [28]. PINK1 accumulates on the mitochondrial outer membrane following the loss of $\Delta\Psi\text{m}$ [29,30] and, in conjunction with Parkin, helps to eliminate damaged mitochondria by autophagy [31–33]. To examine whether the autophagy machinery is involved in the protective effects of p13 knockdown, we evaluated the

mitochondrial accumulation of PINK1 and autophagy induction in rotenone-treated SH-SY5Y cells. We observed that PINK1 accumulation was not stimulated by rotenone regardless of the manipulation of p13 expression (Fig EV3A–C). As shown in Fig EV3D, p13 knockdown did not induce autophagy, as determined by measuring the conversion of LC3-I to LC3-II, which is indicative of autophagic activity [34]. These results suggest that p13 knockdown prevents rotenone-induced mitochondrial dysfunction independently of PINK1-associated autophagy. We found that a mitochondrial uncoupler, carbonyl cyanide *m*-chlorophenylhydrazone (CCCP), but not rotenone, significantly increased PINK1 accumulation (Fig EV3A–C). The underlying mechanism of these results remains unclear, but we found that rotenone mildly reduced $\Delta\Psi\text{m}$ compared to CCCP (Fig EV3E). Since PINK1 accumulates on the mitochondrial outer membrane following the loss of $\Delta\Psi\text{m}$ [19], the rotenone-induced depolarization of $\Delta\Psi\text{m}$ may not be sufficient to trigger PINK1 accumulation. We also found that the CCCP-induced reduction in $\Delta\Psi\text{m}$ was slightly reversed in p13-knockdown cells (Fig EV3F), which is likely to cause the slight decrease in PINK1 accumulation as compared to that in the control-knockdown cells (Fig EV3A). In addition, we found that CCCP treatment did not decrease p13 mRNA levels (Fig EV3G) and that the CCCP-induced decrease in p13 levels was prevented by bafilomycin A1, an autophagy inhibitor (Fig EV3H), suggesting that p13 may be partially degraded by CCCP-mediated autophagy ahead of the other mitochondrial proteins such as Tim23 and Hsp60 (Fig EV3B and C).

Neuronal p13 expression in parkinsonian toxin exposure and PD

We next investigated the *in vivo* function of p13 using an acute MPTP-induced experimental PD model in which nigrostriatal dopaminergic neurons are selectively damaged [15]. Based on an *in situ* hybridization analysis, p13 mRNA was widely expressed in different brain regions, including the olfactory bulb, cortex, hippocampus, cerebellum, striatum and midbrain (Fig EV4A). Western blot analysis indicated that endogenous p13 protein was highly expressed in specific regions, including the cortex, thalamus, midbrain and cerebellum, in mice (Fig EV4C). Using the MPTP-induced PD model, we next examined whether MPTP application changes p13 expression levels in the various regions of the brain. We found that MPTP significantly decreased p13 mRNA expression levels selectively in the midbrain among the examined samples (Fig EV4D). We also found that p13 expression in the midbrain of MPTP-treated mice was decreased compared to that of vehicle-treated mice (Fig EV4E). These data are

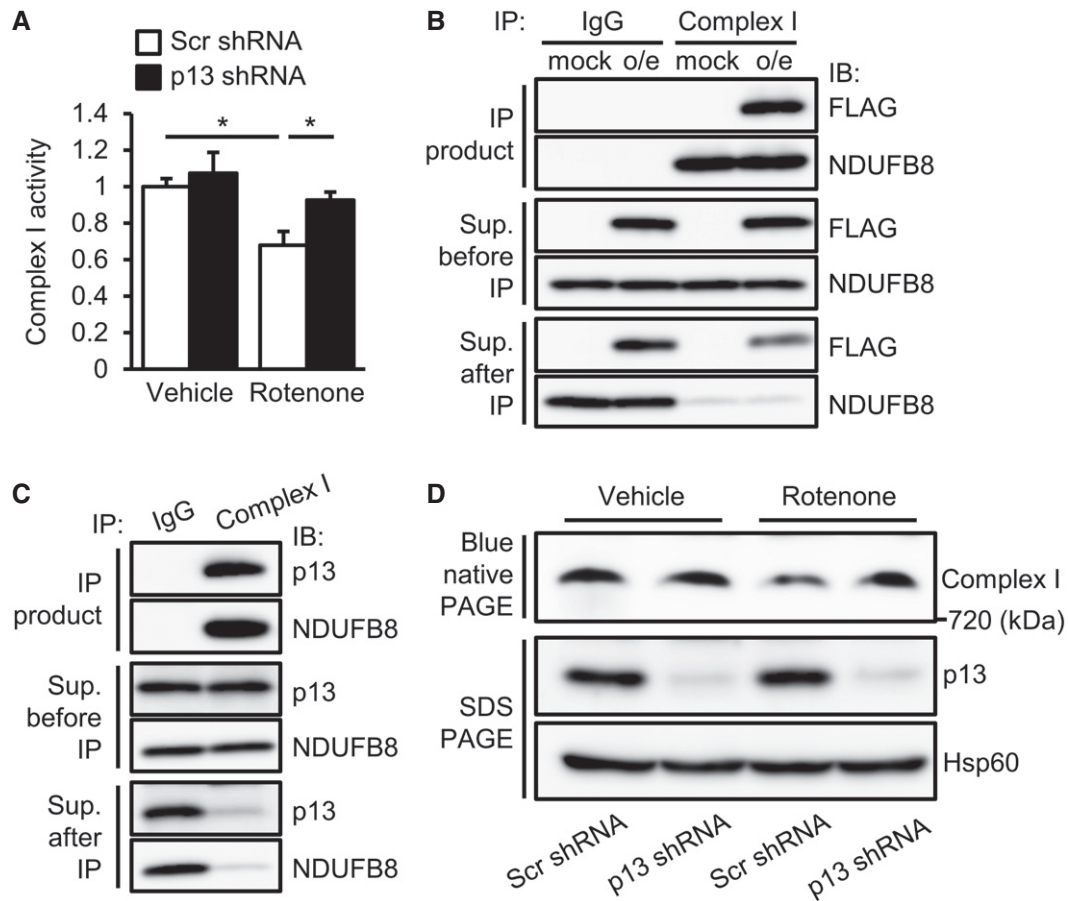


Figure 3. p13 knockdown maintains complex I activity in rotenone-treated SH-SY5Y cells.

- A** Prevention of the rotenone-induced decrease in complex I activity in p13 shRNA-infected cells. Complex I activity was measured on the basis of NADH-oxidizing activity. Data are presented as the mean \pm SEM ($n = 3$). * $P < 0.05$ by the Tukey–Kramer test.
- B, C** Physical interaction between overexpressed p13 (B) or endogenous p13 (C) and complex I proteins. Lysates were immunoprecipitated with anti-complex I antibody and control IgG. The lysates and immunoprecipitates were subjected to Western blotting with antibodies against FLAG (B), p13 (C) or NDUFB8 (complex I protein). Cells were infected with lentiviral vectors expressing mock or FLAG-tagged p13 (p13 o/e, B).
- D** Prevention of rotenone-induced impairment of complex I assembly by p13 knockdown in p13 shRNA-infected cells. Mitochondrial fractions were subjected to blue native PAGE, followed by Western blotting with an antibody against NDUFB8 (complex I protein). Levels of p13 and Hsp60 (for loading control) in the mitochondrial fraction were analysed.

Data information: Seventy-two hours after infection with lentiviral vectors expressing scrambled shRNA (Scr shRNA) or p13 shRNA, cells were stimulated with vehicle or 100 nM rotenone for 24 h (A, D).

consistent with the vulnerability of midbrain dopaminergic neurons to MPTP [15]. Likewise, we observed that rotenone and MPP⁺ decreased the expression of p13 mRNA in SH-SY5Y cells (Fig EV5A and B). While MPP⁺ also decreased the p13 protein levels as well as p13 mRNA levels, rotenone treatment did not decrease p13 protein levels (Fig EV5C and D). The reason for the discrepancy is currently unclear. One possibility is that rotenone may inhibit p13 protein degradation through impairment of lysosomal functions [35]. These results indicate that p13 expression in dopaminergic neurons is decreased by parkinsonian toxicants and suggest that p13 reduction might function as part of an endogenous protective mechanism against PD pathogenesis. Alternatively, many mitochondria proteins are downregulated under toxin-induced conditions [36]; thus, the downregulation of p13 may be a downstream effect of mitochondrial dysfunction. In addition, p13 mRNA expression was not decreased by

rotenone at early time points (2 and 6 h), when the mitochondrial dysfunction determined by the reduction in TMRE intensity was already marked (Fig EV5E and F).

p13 heterozygous knockout prevents MPTP-induced motor deficits and neurodegeneration in mice

To examine the effects of the suppression of p13 expression in an *in vivo* PD model, we generated p13 knockout mice using the CRISPR/Cas9 system (Fig EV6A–D). We used p13^{+/-} mice to evaluate the *in vivo* effects of the p13 knockdown because p13^{-/-} mice showed high lethality shortly after birth (Fig EV6E). We first confirmed that the acute MPTP administration to p13^{+/-} mice caused a marked deficit in motor coordination as measured by rotarod performance (Fig 4A). In sharp contrast to p13^{+/+} mice, p13^{+/-} mice did

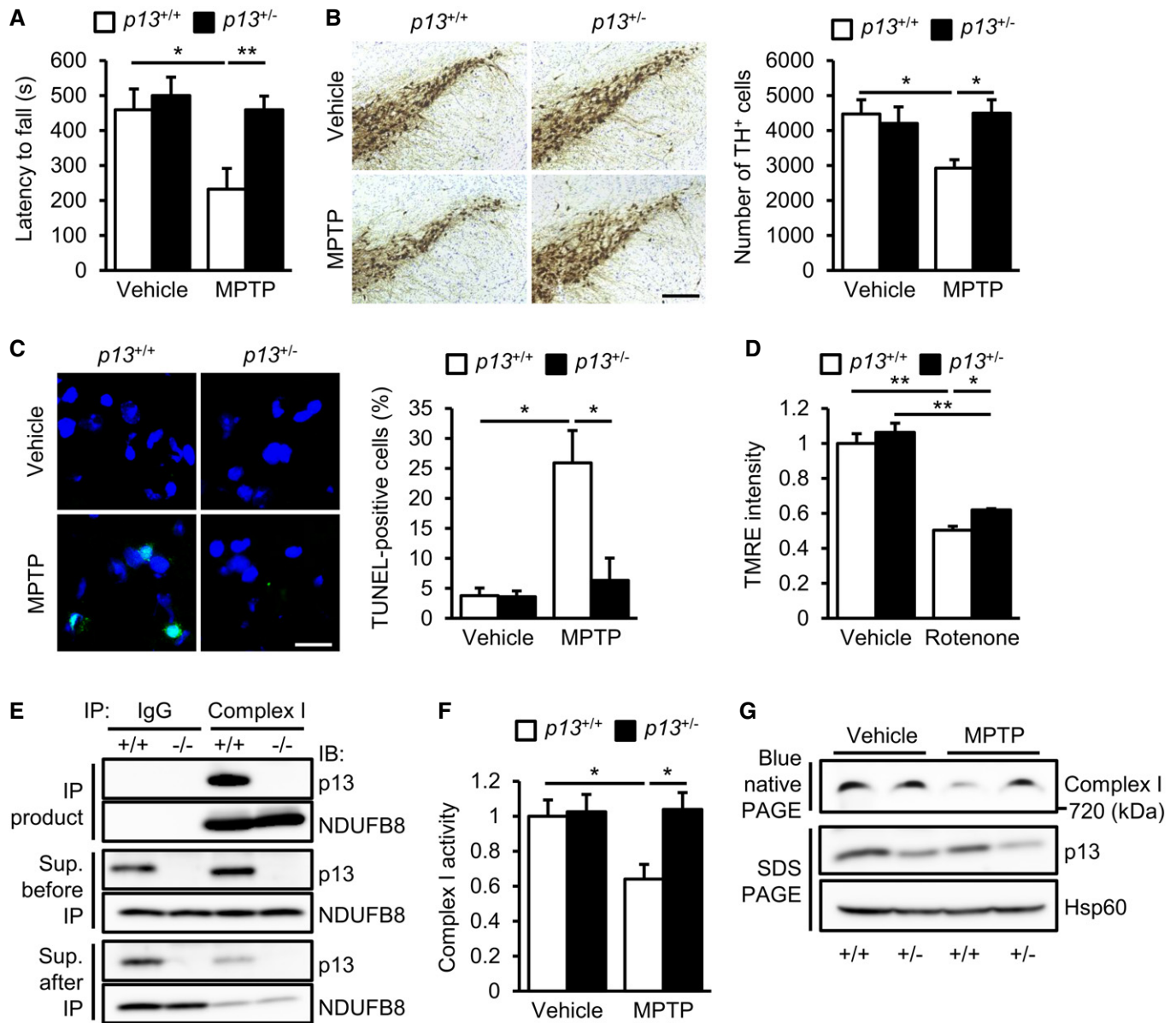


Figure 4. *p13* heterozygous knockout prevents MPTP-induced behavioural deficits and neurodegeneration in mice.

A Prevention of MPTP-induced motor deficits on the rotarod test in $p13^{-/-}$ mice. Latency to fall in two consecutive trials is presented ($n = 10$).

B Prevention of MPTP-induced decrease in TH⁺ neurons in the substantia nigra of $p13^{-/-}$ mice analysed by immunohistochemistry ($n = 4$). Representative images (left) and the quantification of the number of TH⁺ cells in the substantia nigra (right). Scale bar, 200 μ m.

C Prevention of MPTP-induced increase in TUNEL-positive cells in the substantia nigra of $p13^{-/-}$ mice ($n = 3$). Representative images (left, TUNEL, shown in green; Hoechst, shown in blue) and the quantification of percentage of TUNEL-positive cells (right). Scale bar, 20 μ m.

D Attenuation of rotenone-induced decrease in $\Delta\Psi$ m in isolated mitochondria from the midbrain of $p13^{-/-}$ mice ($n = 3$). Isolated mitochondria were exposed to 1 μ M rotenone for 10 min.

E Physical interaction between endogenous p13 and complex I proteins in the brain. Brain extracts from $p13^{+/+}$ and $p13^{-/-}$ mice were immunoprecipitated with anti-complex I antibody and control IgG. The lysates and immunoprecipitates were subjected to Western blotting with antibodies against p13 and NDUFB8 (complex I protein).

F Prevention of the MPTP-induced decrease in complex I activity in the midbrain of $p13^{-/-}$ mice ($n = 3$). Complex I activity was measured on the basis of NADH-oxidizing activity.

G Prevention of MPTP-induced impairment of complex I assembly in the midbrain of $p13^{-/-}$ mice. Mitochondrial fractions were subjected to blue native PAGE, followed by Western blotting with an antibody against NDUFB8 (complex I protein). Levels of p13 and Hsp60 (for loading control) in the mitochondrial fraction were analysed.

Data information: All data are presented as the mean \pm SEM. * $P < 0.05$, ** $P < 0.01$ by the Tukey–Kramer test.

not display MPTP-induced motor deficits (Fig 4A). We then examined the MPTP-induced degeneration of dopaminergic neurons in the substantia nigra of $p13^{+/+}$ and $p13^{+/-}$ mice by using Stereo Investigator software with a fractionator (MBF Bioscience). We found that the MPTP-induced reduction in the number of tyrosine hydroxylase-expressing (TH⁺) cells was almost completely reversed in $p13^{+/-}$ mice compared with $p13^{+/+}$ mice (Fig 4B). In vehicle-treated mice, there was no difference in the number of TH⁺ cells between $p13^{+/+}$ and $p13^{+/-}$ mice (Fig 4B). Furthermore, we measured the optical density of TH⁺ fibres in the striatum and found that MPTP-induced reduction in the optical density of TH⁺ fibres was not reversed in $p13^{+/-}$ mice compared with $p13^{+/+}$ mice (Fig EV6F). As previously reported [37], these results suggest that the restoration of dopaminergic function in the substantia nigra is important for the improvement in MPTP-induced motor dysfunction. Furthermore, we found that the percentage of TUNEL-positive cells was decreased in the substantia nigra of MPTP-treated $p13^{+/-}$ mice (Fig 4C). We also observed that the conversion of LC3 was not induced in the mouse substantia nigra by MPTP regardless of the difference of p13 expression (Fig EV6G). Interestingly, we found that the rotenone-induced decrease in $\Delta\Psi_m$ was slightly attenuated in isolated mitochondria from the midbrain of $p13^{+/-}$ mice (Fig 4D). We found that the endogenous p13 co-precipitated with complex I proteins in the brain samples (Fig 4E). The activity and assembly of mitochondrial complex I in the midbrain of $p13^{+/+}$ mice were impaired by MPTP, whereas those processes were unimpaired in $p13^{+/-}$ mice (Fig 4F and G). These results argue that the targeted knockdown of p13 protects against experimental parkinsonism *in vivo* as well as *in vitro*. In addition, the complex I protein level in the brain of $p13^{-/-}$ mice was virtually identical to that of $p13^{+/+}$ mice (Fig EV6H).

PD is characterized by the progressive and selective degeneration of nigrostriatal dopaminergic neurons, but there is no established neuroprotective or neurorestorative treatment for PD. We demonstrated for the first time that p13 expression was reduced by parkinsonian toxicants both in cell culture and in the mouse midbrain (Figs EV4D and E, and EV5A, B and D). Our mechanistic studies show that p13 knockdown prevented parkinsonian toxicant-induced mitochondrial dysfunction and cell death by enhancing complex I activity (Figs 2C–E and 3A). $p13$ heterozygous knockout also significantly protected mice against MPTP-induced motor deficits and nigral dopaminergic neurodegeneration (Fig 4). Thus, these results suggest that the reduction in p13 expression can act as a protective factor against PD-related pathogenesis and that the manipulation of p13 expression might be a novel and beneficial treatment option for PD.

Controlling mitochondrial integrity has been regarded as a convincing strategy for PD therapeutics [8,9,38]. Indeed, reducing excessive mitochondrial oxidative stress [22,39], stimulating PINK1/Parkin-mediated autophagy [20,40] and promoting mitochondrial biogenesis [41,42] have shown beneficial effects in PD models. However, understanding the PD pathogenesis associated with mitochondria continues to be a major research challenge because mitochondrial function is regulated by a complex network. Our findings suggest that p13 is a novel player in maintaining mitochondrial integrity. Using cell culture and mouse models, our study demonstrates that the reduction in p13 protects dopaminergic cells from mitochondrial dysfunction. Further analyses of the roles of p13

in conjunction with other mitochondrial proteins are important for clarifying the p13-mediated regulation of mitochondrial function in PD pathogenesis. To evaluate the role of p13 in PD pathogenesis, we examined the expression level of $p13$ mRNA in the postmortem brain tissue of three PD patients and three age-matched control subjects. $p13$ mRNA expression levels in the frontal cortex of the patients with PD tended to be lower than those of the control subjects (data not shown); however, the result is necessarily preliminary, mainly owing to the small sample size. The additional therapeutic potential of p13 reduction, such as lack of tolerance or prevention of the disease progression, would be evaluated via further comparative studies using PD patient samples.

On the basis of the present data, the most likely mechanism for the protective effects of p13 reduction against PD pathogenesis is the regulation of complex I activity. p13 has an LYR motif that is associated with the assembly of complex I [43]. We found that p13 physically interacts with complex I proteins (Figs 3B and C, and 4E). A recent study also demonstrated that p13 is likely to interact with NDUFB1, a subunit of complex I [24]. Thus, it is possible that p13 functions as an assembly factor of complex I. In this study, p13 reduction prevented the decrease in complex I activity and assembly by parkinsonian toxicants (Figs 3A and D, and 4F and G). One possible mechanism is that p13 reduction decreases the sensitivity of complex I to parkinsonian toxicants. It remains unclear why 80–90% knockdown of p13 in SH-SY5Y cells had no effect on complex I activity under basal conditions. We found that, in contrast to the heart, there were no significant differences in complex I activity in the brain among $p13^{-/-}$, $p13^{+/-}$ and $p13^{+/+}$ mice (Fig EV6I and J). These results suggest that the importance of p13 function may differ between cell types.

The decreased expression levels of $p13$ mRNA caused by parkinsonian toxicants were comparable to those of p13 shRNA; however, shRNA-mediated p13 knockdown but not parkinsonian toxicant-mediated decreased $p13$ expression protected mitochondrial function against these stresses. The response to decreased $p13$ expression by parkinsonian toxicants may be too late to exert protective effects. Indeed, rotenone rapidly decreased $\Delta\Psi_m$ 2 h after treatment (Fig EV5E), but did not alter $p13$ mRNA levels under the same conditions (Fig EV5F). Considering that mitochondria change their functions early upon stimulation and then promote neurodegeneration, performing p13 knockdown in advance is suggested to be necessary to realize the protective effects of p13 reduction in preventing PD.

In conclusion, we demonstrated that the targeted knockdown of the new mitochondrial protein p13 prevents mitochondrial dysfunction and dopaminergic neuronal death in both *in vitro* and *in vivo* PD models. Our findings should help to explain the molecular pathogenesis of PD. Further studies are needed to propose a new PD therapeutic that targets p13.

Materials and Methods

Cell culture

Human neuroblastoma SH-SY5Y cells were cultured in Dulbecco's modified Eagle's medium (Nissui, Tokyo, Japan) supplemented with 10% foetal bovine serum and 4 mM L-glutamine at 37°C in a

humidified atmosphere of 5% CO₂. Lenti-X 293T cells (Clontech, Mountain View, CA, USA) were maintained in Dulbecco's modified Eagle's medium for lentivirus production.

Lentiviral vectors

Recombinant lentivirus was prepared as described previously [44]. To generate lentiviral vectors expressing mouse p13, mouse cDNA (NP_079639) was amplified via PCR and subcloned into the plasmid CSII-EF-MCS (a generous gift from Dr. Kazuki Nagayasu at Kyoto University). For knockdown experiments, we used a MISSION shRNA construct targeting human p13 (TRCN0000163507, Sigma-Aldrich, St Louis, MO, USA), a non-targeted shRNA control (SHC002, Sigma-Aldrich), another shRNA (p13 shRNA #2) targeting another sequence of p13 (TRCN0000159440, Sigma-Aldrich) and an shRNA construct targeting human PINK1 (TRCN0000199193, Sigma-Aldrich). For rescue experiments, mouse p13 cDNA was subcloned into the MISSION shRNA construct. SH-SY5Y cells were infected with lentiviral vectors at a multiplicity of infection of approximately 20 for overexpression experiments or 40 for knock-down experiments.

Immunocytochemistry

Cells were fixed for 15 min in 4% paraformaldehyde in phosphate-buffered saline (PBS). Permeabilization was performed for 10 min in 0.2% Triton X-100. The cells were blocked for 1 h in 1% bovine serum albumin (BSA, Nacalai Tesque, Kyoto, Japan) in PBS. The cells were then probed with the primary antibodies against p13 (1:250, HPA045663, Atlas Antibodies, Stockholm, Sweden), Hsp60 (1:250, sc-1052, Santa Cruz Biotechnology, Santa Cruz, CA, USA) and complex I proteins (1:500, ab109798, Abcam, Cambridge, UK) overnight at 4°C. Donkey anti-rabbit IgG Alexa Fluor 594 (1:1,000, A-21207, Thermo Fisher Scientific, Tokyo, Japan), donkey anti-goat IgG Alexa Fluor 488 (1:1,000, A-11055, Thermo Fisher Scientific) and donkey anti-mouse IgG Alexa Fluor 488 (1:1,000, A-21202, Thermo Fisher Scientific) antibodies were used as secondary antibodies. Images were acquired with a confocal microscope (FV1000-D, Olympus, Tokyo, Japan).

Mitochondrial toxins

Parkinsonian toxicants rotenone, MPP⁺, MPTP and mitochondrial uncoupler CCCP were purchased from Sigma-Aldrich.

Flow cytometry

Cells were incubated with Opti-MEM[®] (Thermo Fisher Scientific) containing 200 nM TMRE (Thermo Fisher Scientific) or 200 nM MitoTracker Green FM (Thermo Fisher Scientific) for 20 min at 37°C. After trypsinization, cells were resuspended in PBS containing 0.2% BSA, and fluorescence was then detected using a BD Accuri[™] C6 Flow Cytometer (BD Biosciences, San Jose, CA, USA).

Western blotting

Protein samples were resolved by SDS-PAGE and transferred to polyvinylidene fluoride membranes (Millipore, Darmstadt,

Germany). After being blocked with 5% BSA in Tris-buffered saline (TBS) containing 0.1% Tween 20, the membranes were probed with primary antibodies against p13 (1:250), cleaved PARP (1:1,000, 5625S, Cell Signaling, Danvers, MA, USA), β -actin (1:4,000, MAB1501, Chemicon, Temecula, CA, USA), Hsp60 (1:250), Lamin A/C (1:1,000, 2032S, Cell Signaling), Tim23 (1:1,000, 611223, BD Biosciences), GAPDH (1:5,000, 2118S, Cell Signaling), Tom20 (1:1,000, 13929S, Cell Signaling), FLAG (1:1,000, 2368S, Cell Signaling), NDUFB8 (1:2,000, ab110242, Abcam), PINK1 (1:1,000, 6946S, Cell Signaling), LC3 (1:1,000, NB100-2220, Novus Biologicals, Littleton, CO, USA) or NDUFS4 (1:1,000, EPR7831, Abcam) overnight at 4°C. After incubation with the horseradish peroxidase-conjugated secondary antibodies against rabbit IgG (1:2,000, 55689, Cappel, Cochranville, PA, USA), mouse IgG (1:2,000, 55563, Cappel) and goat IgG (1:2,000, 55358, Cappel) for 1 h at room temperature, proteins were detected by chemiluminescence (ImmunoStar Zeta, Wako, Osaka, Japan). Data acquisition and analysis were performed using an LAS 4000 image analyser (GE Healthcare, Piscataway, NJ, USA).

TUNEL staining

TUNEL staining was performed using an *In Situ* Cell Death Detection Kit (Roche Diagnostics, Basel, Switzerland) according to the manufacturer's instruction. Cells were further counterstained with Hoechst. To evaluate the extent of apoptosis, we counted TUNEL-positive cells in five fields per sample for number of TUNEL-positive cells.

Subcellular fractionation and mitochondrial isolation

Subcellular fractionation was performed using FOCUS[™] SubCell Kit (G-Biosciences, Lt. Louis, MO, USA) according to the manufacturer's instruction. Each fraction was determined by Western blotting using the following antibodies: Lamin A/C for nuclear, Tim23 for mitochondrial and GAPDH for cytoplasmic fractions.

For digitonin treatment, blue native PAGE and TMRE staining, mitochondria were isolated according to a previously reported method [45]. Briefly, cells or tissues were homogenized by a Dounce homogenizer in ice-cold IBC buffer (10 mM Tris-MOPS, 1 mM EGTA-Tris, 0.2 M sucrose, pH 7.4). The homogenate was centrifuged at 600 g at 4°C for 10 min, and the supernatant was again centrifuged at 7,000 g at 4°C for 10 min. The precipitated pellets were washed once with IBC buffer. Protein concentration was determined with a BCA Protein Assay Kit (Thermo Fisher Scientific).

Digitonin treatment of isolated mitochondria

Isolated mitochondria were treated with 20 μ g/ml proteinase K in the absence or presence of ascending concentrations of digitonin (0.01, 0.05 and 0.1%) for 10 min, and then, the protease reaction was terminated by the addition of 5 mM phenylmethylsulphonyl fluoride. The mitochondrial extracts were subjected to Western blotting using the following antibodies: p13, Tom20 for the outer mitochondrial membrane, Tim23 for the inner mitochondrial membrane and Hsp60 for the mitochondrial matrix.

Complex I activity assay

Complex I activity was assayed using a complex I enzyme activity microplate assay kit (Abcam). Cell pellets or brain tissues were lysed according to the manufacturer's protocol. A measure of 250 µg protein of each sample was added to each well of the microplate that was pre-coated with anti-complex I antibody, and the microplate was incubated for 3 h at room temperature. After the incubation, complex I activity was determined by monitoring the oxidation of NADH to NAD⁺, coupled to the reporter dye, which leads to increased absorbance at 450 nm. Absorbance was measured by an iMark microplate reader (Bio-Rad, Hercules, CA, USA). The activity was expressed as the change in absorbance per minute.

Co-immunoprecipitation

For the detection of binding between p13 and complex I proteins, SH-SY5Y cells and brains were lysed with a buffer containing 50 mM Tris-HCl (pH 8.0), 100 mM NaCl, 5 mM EDTA, 1% NP-40 and 10 mM NaF. Lysates were incubated with an anti-complex I immunocapture antibody (1:500, Abcam) and protein G-Sepharose (GE Healthcare) overnight at 4°C. Immunocomplexes were washed five times with the buffer, separated by SDS-PAGE and subjected to Western blotting.

Analysis of complex I assembly by blue native PAGE

Mitochondrial proteins (150 µg) were separated on a 3–12% gradient blue native PAGE gel according to the method previously reported [46]. After electrophoresis, the complexes were subjected to Western blotting with an antibody against NDUFB8 for complex I.

Animals

C57BL/6J mice (SLC, Hamamatsu, Japan) were used in this study. Mice were maintained on a 12-h light-dark cycle (lights on at 8:00 a.m.) at a controlled room temperature (22 ± 1°C). Water and food (CMF, Oriental Yeast, Osaka, Japan) were available *ad libitum*. All animal care and handling procedures were approved by the Animal Care and Use Committee of Osaka University. All efforts were made to minimize the number of animals used.

MPTP administration and rotarod test

Mice were subcutaneously administered with MPTP (10 mg/kg) four times at 2-h intervals. Motor performance was assessed by the rotarod test 24 h after the first administration of MPTP, as described previously [37,47,48]. The rotarod (Neuroscience Inc., Tokyo, Japan) consisted of a rotating rod (2.8 cm diameter) and individual compartments for each mouse. Briefly, mice were trained for 3 days prior to MPTP administration in an acceleration mode (2–16 rpm) for over 120 s. The training was repeated at a fixed speed (16 rpm) until the mice were able to stay on the rod for at least 600 s. Motor coordination was measured at a speed of 16 rpm for a maximum recording time of 600 s. Mice were tried twice on 1 day with an interval time of 30 min, and average latency to fall was measured.

Immunohistochemistry

Mice were sacrificed 72 h after the first MPTP administration. Tissue preparation was performed as described previously [49]. Postfixed mouse brains were cut into 20-µm sections containing the substantia nigra (−3.00 to −3.26 mm with respect to bregma) or the striatum (+0.80 through +0.54 mm with respect to bregma) using a cryostat (Leica Biosystems, Tokyo, Japan). Sections were incubated for 30 min in 0.3% hydrogen peroxide in PBS and then blocked with 1% normal goat serum (Vectastain ABC HRP kit; Vector Laboratories, Burlingame, CA, USA) in PBS for 1 h at room temperature. The sections were incubated with the antibody against TH (1:1,000, AB152, Millipore) in PBS containing 1% normal goat serum and 0.1% Triton X-100 overnight at 4°C. Subsequently, sections were incubated in a secondary antibody solution containing biotinylated anti-rabbit IgG (1:125, Vectastain ABC HRP kit; Vector Laboratories) in PBS for 30 min at room temperature and then reacted with the avidin-biotin peroxidase complex (1:125, Vectastain ABC HRP kit; Vector Laboratories) in PBS for 30 min at room temperature. Visualization was performed using a DAB substrate kit (Nichirei Corporation, Tokyo, Japan) according to the manufacturer's protocol. Penetration was conducted with ethanol (95 and 100%) and xylene. Sections were also counterstained by Nissl staining. Images were acquired with a microscope (BZ-9000, Keyence, Osaka, Japan). The total number of TH⁺ neurons in every fourth section of the substantia nigra was counted stereologically with Stereo Investigator software (MBF Bioscience, Williston, VT, USA) using the fractionator method.

TMRE staining in isolated mitochondria from mice

Isolated mitochondria from the mouse midbrain were stained with TMRE as described previously [50]. Briefly, isolated mitochondria (75 µg) were incubated with EB buffer (125 mM KCl, 10 mM Tris-MOPS, 5 mM glutamate, 2.5 mM malate, 1 mM K phosphate and 10 mM EGTA-Tris, pH 7.4) containing 1 µM TMRE for 10 min at room temperature. The homogenate was centrifuged at 10,000 g at 4°C for 5 min. The precipitated pellets were resuspended with the EB buffer, and fluorescence was then detected using a Spectramax M5e (Molecular Devices, Sunnyvale, CA, USA).

Real-time RT-PCR

Total RNA was isolated using QIAzol Lysis Reagent (QIAGEN, Tokyo, Japan) according to the manufacturer's protocol. Reverse transcription of total RNA (1 µg) and real-time RT-PCR were performed as described previously [51]. Real-time RT-PCR was conducted with GoTaq qPCR Master Mix (Promega, Madison, WI, USA). The primer sequences were as follows:

Human p13_forward, 5'-AAGGCTTTCGGTGCACATCGG-3'
Human p13_reverse, 5'-CAGCCCTCCCTCCAGGCTGAT-3'
Human β-actin_forward, 5'-CATGTGCAAGCCGGCTCG-3'
Human β-actin_reverse, 5'-CTGGTCATCTCTCGCGGT-3'
Human PINK1_forward, 5'-GCCATCAAGATGATGTGGAAC-3'
Human PINK1_reverse, 5'-GACCAGCTCCTGGCTCATT-3'
Human ND1_forward, 5'-CACCTCTAGCCTAGCCGTTT-3'
Human ND1_reverse, 5'-CCGATCAGGGCGTAGTTTGA-3'

Human ND2_forward, 5'-CTTAAACTCCAGCACCACGAC-3'
 Human ND2_reverse, 5'-AGCTTGTTCAGGTGCGAGA-3'
 Human ND3_forward, 5'-CCGCGTCCCTTTCTCCATAA-3'
 Human ND3_reverse, 5'-AGGGCTCATGGTAGGGGTAA-3'
 Human ND4_forward, 5'-ACAACACAATGGGGCTCACT-3'
 Human ND4_reverse, 5'-CCGGTAATGATGTCGGGGTT-3'
 Human ND4L_forward, 5'-TCGCTCACACCTCATATCCTC-3'
 Human ND4L_reverse, 5'-AGGCGCAAAGACTAGTATGG-3'
 Human ND5_forward, 5'-TCCATTGTCGCATCCACCTT-3'
 Human ND5_reverse, 5'-GGTTGTTGGGTTGTGGCTC-3'
 Human ND6_forward, 5'-GGGTTGAGGCTCTGGTGAGT-3'
 Human ND6_reverse, 5'-ACCAATCCTACCTCCATCGC-3'
 Human CYTB_forward, 5'-TCTTGCACGAAACGGGATCA-3'
 Human CYTB_reverse, 5'-CGAGGGCGTCTTTGATTGTG-3'
 Human COX1_forward, 5'-TCCTTATTCGAGCCGAGCTG-3'
 Human COX1_reverse, 5'-ACAAATGCATGGGCTGTGAC-3'
 Human COX2_forward, 5'-AACCAACCCTTTCACCGC-3'
 Human COX2_reverse, 5'-CGATGGGCATGAACTGTGG-3'
 Human ATP6_forward, 5'-TTCGCTTCATTCATTGCCCC-3'
 Human ATP6_reverse, 5'-GGTGTTGATTAGTCGGTTGT-3'
 Human ATP8_forward, 5'-ACTACCACCTACCTCCCTCAC-3'
 Human ATP8_reverse, 5'-GGCAATGAATGAAGCGAACAGA-3'
 Mouse p13_forward, 5'-AAGGCTTTCGTCACATCGG-3'
 Mouse p13_reverse, 5'-CAGCCCTTCCCTCCAGGCTGAC-3'
 Mouse β -actin_forward, 5'-ACCCACACTGTGCCCATCTA-3'
 Mouse β -actin_reverse, 5'-GCCACAGGATTCCATACCCA-3'

LDH assay

LDH levels released from damaged cells were measured using a cytotoxicity detection kit (Roche Diagnostics) according to the manufacturer's protocol. The culture medium of the cells was incubated with the reaction mixture at room temperature for 30 min. Signals at wavelengths of 490 and 620 nm were measured by spectrophotometry.

In situ hybridization

In situ hybridization analysis was performed on sagittal brain sections as described previously [52]. Complementary DNA fragments encoding mouse *p13* cDNA (NP_079639) were used as templates to synthesize [³⁵S] CTP-labelled cRNA probes.

CRISPR/Cas9-based knockout of *p13* in mice

p13 knockout mice were generated using the CRISPR/Cas9 system. The sgRNA sequences 5'-GACAGAAAAATGGCGGCCCT-3' and 5'-CGTACTCTGAACGCGGCCAC-3' targeting exon 1 of the mouse *p13* gene were cloned into pX330 (Addgene, Cambridge, MA, USA). pCAG-EGFP was used to examine the efficiency of the target DNA cleavage by the gRNAs and Cas9 [53]. The pX330 plasmids containing each sgRNA sequence were injected into the pronuclear stage eggs. Mice that harboured a 71-bp deletion in exon 1 of the *p13* gene were obtained. The genotypes of all mice were analysed by PCR for a mutated *p13* locus using the following primers:

Genotyping primer p13_forward, 5'-CACCTTCCCTTGTCTCCTG-3'
 Genotyping primer p13_reverse, 5'-GAGACCCTCTATCACCTGCG-3'

Data analysis and statistics

Statistical analysis was performed using Statview (SAS Institute Japan Ltd., Tokyo, Japan), and significant differences were determined by Student's *t*-test, Dunnett's test and the Tukey–Kramer test. The threshold for statistical significance was defined as $P < 0.05$.

Expanded View for this article is available online.

Acknowledgements

We thank NPO Biotechnology Research and Development for technical assistance. We are grateful to Dr. Koji Okamoto (Osaka University) for helpful discussions. This work was supported in part by the Japan Society for the Promotion of Science (JSPS) KAKENHI grant numbers JP25670038 (NS), JP17H03989 (HH), JP17K19488 (HH) and JP26293020 (HH); Project MEET, Osaka University Graduate School of Medicine (NS); Mitsubishi Tanabe Pharma Corporation (NS); the JSPS Program for Advancing Strategic International Networks to Accelerate the Circulation of Talented Researchers, grant number S2603 (HH); the SRPBS and Brain/MINDS from AMED (HH); JSPS Research Fellowships for Young Scientists, grant number JP15J06322 (NI); and grants for research from the Uehara Memorial Foundation, Japan (NS).

Author contributions

NI, SO, KI, SH and YS performed experiments. NI, SO and AI generated *p13*-deficient mice. KB, HM and HF assessed *p13* mRNA levels in autopsied brain tissues. NI, SO, AK, TN, YA, AH-T, KS, NS and HH analysed the data. AK, TN, HM, YA, AH-T, KS, NS and HH provided guidance and/or senior supervision. NI, AK, TN, NS and HH wrote the manuscript. NI and SO prepared the figures under supervision from AK, TN, NS and HH. All authors provided input and corrections to the preparation of the manuscript and figures.

Conflict of interest

The authors declare that they have no conflict of interest.

References

- Berg D, Postuma RB, Bloem B, Chan P, Dubois B, Gasser T, Goetz CG, Halliday GM, Hardy J, Lang AE et al (2014) Time to redefine PD? Introductory statement of the MDS Task Force on the definition of Parkinson's disease. *Mov Disord* 29: 454–462
- Postuma RB, Berg D, Stern M, Poewe W, Olanow CW, Oertel W, Obeso J, Marek K, Litvan I, Lang AE et al (2015) MDS clinical diagnostic criteria for Parkinson's disease. *Mov Disord* 30: 1591–1601
- Jenner P (2008) Molecular mechanisms of L-DOPA-induced dyskinesia. *Nat Rev Neurosci* 9: 665–677
- Athauda D, Foltynie T (2015) The ongoing pursuit of neuroprotective therapies in Parkinson disease. *Nat Rev Neurol* 11: 25–40
- Kalia LV, Kalia SK, Lang AE (2015) Disease-modifying strategies for Parkinson's disease. *Mov Disord* 30: 1442–1450
- Choong CJ, Baba K, Mochizuki H (2016) Gene therapy for neurological disorders. *Expert Opin Biol Ther* 16: 143–159
- Ryan BJ, Hoek S, Fon EA, Wade-Martins R (2015) Mitochondrial dysfunction and mitophagy in Parkinson's: from familial to sporadic disease. *Trends Biochem Sci* 40: 200–210
- Schon EA, Przedborski S (2011) Mitochondria: the next (neurode)generation. *Neuron* 70: 1033–1053

9. Exner N, Lutz AK, Haass C, Winklhofer KF (2012) Mitochondrial dysfunction in Parkinson's disease: molecular mechanisms and pathophysiological consequences. *EMBO J* 31: 3038–3062
10. Choong CJ, Mochizuki H (2017) Gene therapy targeting mitochondrial pathway in Parkinson's disease. *J Neural Transm* 124: 193–207
11. Hattori N, Ikebe S, Tanaka M, Ozawa T, Mizuno Y (1993) Immunohistochemical studies on complexes I, II, III, and IV of mitochondria in Parkinson's disease. *Adv Neurol* 60: 292–296
12. Mizuno Y, Ohta S, Tanaka M, Takamiya S, Suzuki K, Sato T, Oya H, Ozawa T, Kagawa Y (1989) Deficiencies in complex I subunits of the respiratory chain in Parkinson's disease. *Biochem Biophys Res Commun* 163: 1450–1455
13. Schapira AH, Cooper JM, Dexter D, Clark JB, Jenner P, Marsden CD (1990) Mitochondrial complex I deficiency in Parkinson's disease. *J Neurochem* 54: 823–827
14. Betarbet R, Sherer TB, MacKenzie G, Garcia-Osuna M, Panov AV, Greenamyre JT (2000) Chronic systemic pesticide exposure reproduces features of Parkinson's disease. *Nat Neurosci* 3: 1301–1306
15. Dauer W, Przedborski S (2003) Parkinson's disease: mechanisms and models. *Neuron* 39: 889–909
16. Porras G, Li Q, Bezaud E (2012) Modeling Parkinson's disease in primates: the MPTP model. *Cold Spring Harb Perspect Med* 2: a009308
17. Manfredi G (2006) mtDNA clock runs out for dopaminergic neurons. *Nat Genet* 38: 507–508
18. Schapira AH (2008) Mitochondria in the aetiology and pathogenesis of Parkinson's disease. *Lancet Neurol* 7: 97–109
19. Martinez-Vicente M (2017) Neuronal mitophagy in neurodegenerative diseases. *Front Mol Neurosci* 10: 64
20. Pickrell AM, Youle RJ (2015) The roles of PINK1, parkin, and mitochondrial fidelity in Parkinson's disease. *Neuron* 85: 257–273
21. Higashi S, Katagi K, Shintani N, Ikeda K, Sugimoto Y, Tsuchiya S, Inoue N, Tanaka S, Koumoto M, Kasai A et al (2015) p13 overexpression in pancreatic beta-cells ameliorates type 2 diabetes in high-fat-fed mice. *Biochem Biophys Res Commun* 461: 612–617
22. Lin MT, Beal MF (2006) Mitochondrial dysfunction and oxidative stress in neurodegenerative diseases. *Nature* 443: 787–795
23. Ott M, Gogvadze V, Orrenius S, Zhivotovskiy B (2007) Mitochondria, oxidative stress and cell death. *Apoptosis* 12: 913–922
24. Floyd BJ, Wilkerson EM, Veling MT, Minogue CE, Xia C, Beebe ET, Wrobel RL, Cho H, Kremer LS, Alston CL et al (2016) Mitochondrial protein interaction mapping identifies regulators of respiratory chain function. *Mol Cell* 63: 621–632
25. Han S, Udeshi ND, Deerinck TJ, Svinkina T, Ellisman MH, Carr SA, Ting AY (2017) Proximity biotinylation as a method for mapping proteins associated with mtDNA in living cells. *Cell Chem Biol* 24: 404–414
26. Galluzzi L, Blomgren K, Kroemer G (2009) Mitochondrial membrane permeabilization in neuronal injury. *Nat Rev Neurosci* 10: 481–494
27. Kroemer G, Galluzzi L, Brenner C (2007) Mitochondrial membrane permeabilization in cell death. *Physiol Rev* 87: 99–163
28. Yamano K, Matsuda N, Tanaka K (2016) The ubiquitin signal and autophagy: an orchestrated dance leading to mitochondrial degradation. *EMBO Rep* 17: 300–316
29. Matsuda N, Sato S, Shiba K, Okatsu K, Saisho K, Gautier CA, Sou YS, Saiki S, Kawajiri S, Sato F et al (2010) PINK1 stabilized by mitochondrial depolarization recruits Parkin to damaged mitochondria and activates latent Parkin for mitophagy. *J Cell Biol* 189: 211–221
30. Narendran DP, Jin SM, Tanaka A, Suen DF, Gautier CA, Shen J, Cookson MR, Youle RJ (2010) PINK1 is selectively stabilized on impaired mitochondria to activate Parkin. *PLoS Biol* 8: e1000298
31. Kazlauskaite A, Martinez-Torres RJ, Wilkie S, Kumar A, Peltier J, Gonzalez A, Johnson C, Zhang J, Hope AG, Pegg M et al (2015) Binding to serine 65-phosphorylated ubiquitin primes Parkin for optimal PINK1-dependent phosphorylation and activation. *EMBO Rep* 16: 939–954
32. Narendran D, Tanaka A, Suen DF, Youle RJ (2008) Parkin is recruited selectively to impaired mitochondria and promotes their autophagy. *J Cell Biol* 183: 795–803
33. Twig G, Elorza A, Molina AJ, Mohamed H, Wikstrom JD, Walzer G, Stiles L, Haigh SE, Katz S, Las G et al (2008) Fission and selective fusion govern mitochondrial segregation and elimination by autophagy. *EMBO J* 27: 433–446
34. Kabeya Y, Mizushima N, Ueno T, Yamamoto A, Kirisako T, Noda T, Komiyama E, Ohsumi Y, Yoshimori T (2000) LC3, a mammalian homologue of yeast Apg8p, is localized in autophagosomal membranes after processing. *EMBO J* 19: 5720–5728
35. Wu F, Xu HD, Guan JJ, Hou YS, Gu JH, Zhen XC, Qin ZH (2015) Rotenone impairs autophagic flux and lysosomal functions in Parkinson's disease. *Neuroscience* 284: 900–911
36. Zheng B, Liao Z, Locascio JJ, Lesniak KA, Roderick SS, Watt ML, Eklund AC, Zhang-James Y, Kim PD, Hauser MA et al (2010) PGC-1 α , a potential therapeutic target for early intervention in Parkinson's disease. *Sci Transl Med* 2: 52ra73
37. Kawasaki T, Ishihara K, Ago Y, Baba A, Matsuda T (2007) Edaravone (3-methyl-1-phenyl-2-pyrazolin-5-one), a radical scavenger, prevents 1-methyl-4-phenyl-1,2,3,6-tetrahydropyridine-induced neurotoxicity in the substantia nigra but not the striatum. *J Pharmacol Exp Ther* 322: 274–281
38. Andreux PA, Houtkooper RH, Auwerx J (2013) Pharmacological approaches to restore mitochondrial function. *Nat Rev Drug Discov* 12: 465–483
39. Jin H, Kanthasamy A, Ghosh A, Anantharam V, Kalyanaraman B, Kanthasamy AG (2014) Mitochondria-targeted antioxidants for treatment of Parkinson's disease: preclinical and clinical outcomes. *Biochim Biophys Acta* 1842: 1282–1294
40. Yasuda T, Hayakawa H, Nihira T, Ren YR, Nakata Y, Nagai M, Hattori N, Miyake K, Takada M, Shimada T et al (2011) Parkin-mediated protection of dopaminergic neurons in a chronic MPTP-minipump mouse model of Parkinson disease. *J Neuropathol Exp Neurol* 70: 686–697
41. Hasegawa K, Yasuda T, Shiraishi C, Fujiwara K, Przedborski S, Mochizuki H, Yoshikawa K (2016) Promotion of mitochondrial biogenesis by necdin protects neurons against mitochondrial insults. *Nat Commun* 7: 10943
42. Mudo G, Makela J, Di Liberto V, Tselikh TV, Olivieri M, Piepponen P, Eriksson O, Malkia A, Bonomo A, Kairisalo M et al (2012) Transgenic expression and activation of PGC-1 α protect dopaminergic neurons in the MPTP mouse model of Parkinson's disease. *Cell Mol Life Sci* 69: 1153–1165
43. Angerer H (2015) Eukaryotic LYR proteins interact with mitochondrial protein complexes. *Biology* 4: 133–150
44. Hashimoto R, Nakazawa T, Tsurusaki Y, Yasuda Y, Nagayasu K, Matsumura K, Kawashima H, Yamamori H, Fujimoto M, Ohi K et al (2016) Whole-exome sequencing and neurite outgrowth analysis in autism spectrum disorder. *J Hum Genet* 61: 199–206
45. Frezza C, Cipolat S, Scorrano L (2007) Organelle isolation: functional mitochondria from mouse liver, muscle and cultured fibroblasts. *Nat Protoc* 2: 287–295
46. Jha P, Wang X, Auwerx J (2016) Analysis of mitochondrial respiratory chain supercomplexes using blue native polyacrylamide gel electrophoresis (BN-PAGE). *Curr Protoc Mouse Biol* 6: 1–14
47. Ago Y, Kawasaki T, Nashida T, Ota Y, Cong Y, Kitamoto M, Takahashi T, Takuma K, Matsuda T (2011) SEA0400, a specific Na⁺/Ca²⁺ exchange

- inhibitor, prevents dopaminergic neurotoxicity in an MPTP mouse model of Parkinson's disease. *Neuropharmacology* 61: 1441–1451
48. Kawasaki T, Ago Y, Kitao T, Nashida T, Takagi A, Takuma K, Matsuda T (2008) A neuroprotective agent, T-817MA (1-{3-[2-(1-benzothiophen-5-yl)ethoxy]propyl} azetidin-3-ol maleate), prevents 1-methyl-4-phenyl-1,2,3,6-tetrahydropyridine-induced neurotoxicity in mice. *Neuropharmacology* 55: 654–660
49. Seiriki K, Kasai A, Kuwaki T, Nakazawa T, Yamaguchi S, Hashimoto H (2016) Critical involvement of the orbitofrontal cortex in hyperlocomotion induced by NMDA receptor blockade in mice. *Biochem Biophys Res Commun* 480: 558–563
50. Lampl T, Crum JA, Davis TA, Milligan C, Del Gaizo Moore V (2015) Isolation and functional analysis of mitochondria from cultured cells and mouse tissue. *J Vis Exp* 97: e52076
51. Yamasaki A, Kasai A, Toi A, Kurita M, Kimoto S, Hayata-Takano A, Nakazawa T, Nagayasu K, Shintani N, Hashimoto R et al (2015) Identification of the role of bone morphogenetic protein (BMP) and transforming growth factor-beta (TGF-beta) signaling in the trajectory of serotonergic differentiation in a rapid assay in mouse embryonic stem cells *in vitro*. *J Neurochem* 132: 418–428
52. Hashimoto H, Nogi H, Mori K, Ohishi H, Shigemoto R, Yamamoto K, Matsuda T, Mizuno N, Nagata S, Baba A (1996) Distribution of the mRNA for a pituitary adenylate cyclase-activating polypeptide receptor in the rat brain: an *in situ* hybridization study. *J Comp Neurol* 371: 567–577
53. Mashiko D, Fujihara Y, Satouh Y, Miyata H, Isotani A, Ikawa M (2013) Generation of mutant mice by pronuclear injection of circular plasmid expressing Cas9 and single guided RNA. *Sci Rep* 3: 3355